pp. 1–13 (2020)

# Spatially averaged haemodynamic models for different parts of cardiovascular system

S. S. Simakov*

**Abstract** — This paper revisits the usage of spatially averaged haemodynamic models such as non-stationary 1D/0D in space and stationary 0D in space models. Conditions of equivalence between different 1D model formulations are considered. The impact of circular and elliptic shapes of the tube cross-section on the friction term and the tube law is analyzed. Finally, the relationship between 0D lumped and 1D models is revealed.

**Keywords:** 1D haemodynamic model, 0D lumped model, blood flow

**MSC 2010:** 65D25, 37M05, 92B99

The choice of blood flow modelling method depends on the time-to-time variability of the flow, the spatial scale of the vascular domain and the target physiological and pathological processes. The most detailed are 3D models which consider the interaction of flow with a moving viscoelastic vascular wall (FSI) [25, 45]. The 3D FSI modelling is a complicated task both from technological and practical points of view. It requires to specify with great details 3D geometry of the vascular region, elastic properties of the wall, boundary conditions, and to apply advanced numerical schemes.

This paper revisits the usage of spatially averaged haemodynamic models such as non-stationary 1D/0D in space and stationary 0D in space models. They are useful for analysis of blood flow in vascular networks including tens or hundreds of vessels. These models are also applied to modelling the closed-loop circulation including systemic and pulmonary arteries and veins via 1D [1, 6, 7, 28, 39] and 0D [10, 17, 23] reductions. Detailed descriptions of spatially averaged blood flow models can be found in [4, 32, 36, 40, 45, 46], although some issues (e.g. blood flow in veins) have received less attention. In this work we present a monolithic view to reduced-order blood flow in different parts of the cardiovascular system.

Methods of the reduced-order solution of FSI problems include two basic ideas: asymptotic analysis with a thin wall assumption [2, 9, 15, 18] and integration over a

*Moscow Institute of Physics and Technology, Dolgoprudny 141700, Russia; Sechenov University, Moscow 119991, Russia. E-mail: simakov.ss@mipt.ru

The research was supported by the Russian Foundation for Basic Research (grant Nos. 18-00-01524, 18-31-20048, 18-00-01661) and Moscow Center for Fundamental and Applied Mathematics (agreement with the Ministry of Education and Science of the Russian Federation No. 075-15-2019-1624).

cross-section of an elastic tube [11]. We apply the spatial averaging procedure [11] to the Navier–Stokes equations for flows of viscous incompressible fluid in long elastic tubes with circular cross-section and study some specific details which are not addressed in the literature. The derivation gives 1D equations for the cross-section area and flow variables. In particular, a 1D formulation using the cross-section and averaged linear velocity variables provides a system of hyperbolic equations. Numerical methods for the approximate solution of such system are well known. Thus first, we consider in details conditions of equivalence between different 1D model formulations. Flows in the elastic tubes with circular and elliptic cross-section are different, and the model of the blood flow in veins should be studied separately. Second, we consider the impact of circular and elliptic cross-sections on the friction term and the tube law contributing to 1D haemodynamic models. Spatial and/or dynamic effects may be neglected in some parts of the cardiovascular system where 0D lumped models may be used successfully (microcirculation, heart chambers); therefore, we clarify the relationship between 0D lumped and 1D models.

The rest of the paper is organized as follows. In Section 1 we consider 1D haemodynamic models in large arteries (Section 1.1) and veins (Section 1.2). In Section 2 we derive spatially averaged 0D lumped models which describe variations of pressure, volume and flow in time (Section 2.1) and time-averaged relationships between them (Section 2.2). Concluding remarks are given in Section 3.

## 1. 1D haemodynamic models in large vessels

The Reynolds number in arteries ranges from 10 to $4 \cdot 10^3$. The standard assumptions for deriving 1D hemodynamic models are:

1. The ratio of the vessel diameter to its length is small.
2. The shape of the velocity profile in any cross-section orthogonal to the vessel centerline remains the same along the centerline (e.g., it stays flat or parabolic).
3. The pressure is constant in each cross-section.
4. The forces act on the vessel wall in normal directions and wall displacements occur in the same direction.

The detailed list can be found in [45].

### 1.1. 1D haemodynamic model for large arteries

The above assumptions allow us to integrate the 3D Navier–Stokes equations over a cross-sectional slice [11,45]. We consider a slice of an elastic tube (vessel) between two cross sections $\Gamma_1$ and $\Gamma_2$ orthogonal to its centerline (see Fig. 1 for the 2D analogue). Here $\Gamma_W$ is tube wall, $\Omega$ is the integration domain limited by $\Gamma_1 \cup \Gamma_2 \cup$

$\Gamma_W$. Let $t$ be the time, $x$ denote the coordinate along the centerline, $\Gamma_S$ be a circular cross-section orthogonal to the centerline at a point with coordinate $x$, the radius of $\Gamma_S$ be $R(t,x)$ and the area be $S(t,x) = \pi R^2(t,x)$, $\eta(t,x)$ be the displacement of the wall in the radial direction of $\Gamma_S$. In the cross-section we introduce the radial coordinate $r$ and the Cartesian coordinates $y$, $z$.

Due to the assumptions, the Navier–Stokes equations for the incompressible Newtonian viscous fluid are reduced to

$$\operatorname{div}\mathbf{u} = 0 \tag{1.1}$$

$$\frac{\partial u_x}{\partial t} + \operatorname{div}(u_x\mathbf{u}) + \frac{1}{\rho}\frac{\partial P}{\partial x} - \nu\Delta u_x = 0 \tag{1.2}$$

$$u_x(t,x,y,z) = \bar{u}(t)\xi(x,y,z) \tag{1.3}$$

$$u_r(t,R,x) = \frac{\partial \eta}{\partial t}(t,x) \tag{1.4}$$

where $\mathbf{u} = (u_x, u_y, u_z)$ is the 3D velocity, $P(t,x)$ is the pressure, $\rho = 1.04\,\mathrm{g/cm^3}$ is the blood density, $\nu = 0.04\,\mathrm{cm^2/s}$ is the blood viscosity. The shape of the velocity profile in (1.3) is defined by function

$$\xi(x,y,z) = \frac{\gamma+2}{\gamma}\left(1 - \left(\frac{y^2+z^2}{R^2(t,x)}\right)^{\gamma/2}\right), \quad y^2+z^2 \leqslant R^2(t,x). \tag{1.5}$$

Here $\gamma = 2$ corresponds to the parabolic (Poiseuille) profile, $\gamma = 9$ corresponds to an almost flat profile. Equation (1.4) means the non-slip condition on the side wall $\Gamma_W$ since $u_x(t,R,x) = 0$ due to assumption 4. In (1.3) we define the linear velocity averaged in $\Gamma_S$ as

$$u = \frac{1}{S}\int\limits_{\Gamma_S} u_x \mathrm{d}s. \tag{1.6}$$

We will also use the flow $Q$ through the cross-section $\Gamma_S$ as

$$Q|_{\Gamma_S} = \int\limits_{\Gamma_S} u_x \mathrm{d}s = Su. \tag{1.7}$$

Integrating incompressibility equation (1.1) over $\Omega$ we get

$$0 = \int\limits_{\Omega} \operatorname{div}\mathbf{u}\mathrm{d}\mathbf{x} = \int\limits_{\partial\Omega} \mathbf{u}\cdot\mathbf{n}\mathrm{d}s = \int\limits_{\Gamma_2} u_x\mathrm{d}s - \int\limits_{\Gamma_1} u_x\mathrm{d}s + \int\limits_{\Gamma_W} u_r\mathrm{d}s \tag{1.8}$$

which is transformed into the 1D mass conservation equation

$$\frac{\partial S}{\partial t} + \frac{\partial Q}{\partial x} = 0. \tag{1.9}$$

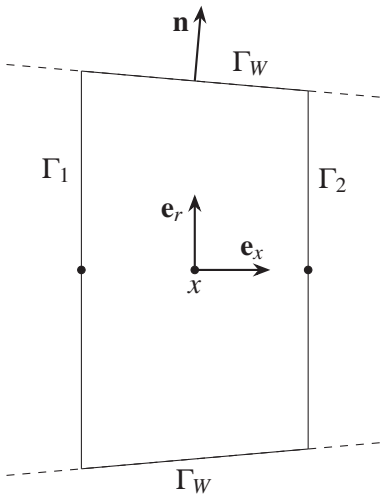


**Figure 1.** Integration domain (2D case).

Integrating momentum equation (1.2) over $\Omega$ we get

$$\int_\Omega \frac{\partial u_x}{\partial t}\mathrm{d}\mathbf{x} + \int_\Omega \mathrm{div}\,(u_x\mathbf{u})\mathrm{d}\mathbf{x} + \frac{1}{\rho}\int_\Omega \frac{\partial P}{\partial x}\mathrm{d}\mathbf{x} - \nu\int_\Omega \Delta u_x \mathrm{d}\mathbf{x} = 0 \tag{1.10}$$

which is transformed into the 1D momentum conservation equation

$$\frac{\partial Q}{\partial t} + \frac{\partial}{\partial x}\left(\alpha\frac{Q^2}{S}\right) + \frac{S}{\rho}\frac{\partial P}{\partial x} = K_r u \tag{1.11}$$

where

$$K_r = -2\pi(\gamma+2)\nu \tag{1.12}$$

$$\alpha = \frac{1}{Su^2}\int_{\Gamma_S} u^2\mathrm{d}s = \pi^{-1}R^{-2}u^{-2}\int_0^R \left(\frac{\gamma+2}{\gamma}\right)^2 \bar{u}^2\left(1-\frac{r^\gamma}{R^\gamma}\right)^2 2\pi r\,\mathrm{d}r = \frac{\gamma+2}{\gamma+1}. \tag{1.13}$$

Substituting $Q = Su$ to (1.9) and (1.11) we get

$$\frac{\partial S}{\partial t} + \frac{\partial(Su)}{\partial x} = 0 \tag{1.14}$$

$$\frac{\partial u}{\partial t} + \left(\alpha - \frac{1}{2}\right)\frac{\partial u^2}{\partial x} + (\alpha-1)\frac{u^2}{S}\frac{\partial S}{\partial x} + \frac{1}{\rho}\frac{\partial P}{\partial x} = -2\pi(\gamma+2)\nu\frac{u}{S}. \tag{1.15}$$

The third equation of the model is a constitutive relationship between $P$ and $S$ which defines the elastic properties of the tube wall. It describes the response of collagen and elastin fibres of the vessel to the pressure difference across the wall

(transmural pressure). This relationship is also known as the tube law. For arteries, its general form [44] is

$$P = F(S) \tag{1.16}$$

where $F(S)$ is a smooth monotonic function with $\partial F/\partial S > 0$. Since the inverse function $S = \hat{F}(P)$ exists and $\partial \hat{F}/\partial P > 0$, equation (1.15) transforms to

$$\frac{\partial u}{\partial t} + \left(\alpha - \frac{1}{2}\right)\frac{\partial u^2}{\partial x} + \left(1 + (\alpha - 1)\frac{\rho u^2}{S}\frac{\partial \hat{F}}{\partial P}\right)\frac{1}{\rho}\frac{\partial P}{\partial x} = \psi \tag{1.17}$$

where $\psi = -2\pi(\gamma+2)\nu u S^{-1}$.

If one chooses the tube law $F(S) = P_{\text{ext}} + \rho_w c_0^2\left(e^{S/S_0 - 1} - 1\right)$ for $S_0$ denoting the cross-section area under $P = 0$ [39, 40, 44], he gets $\hat{F} = \left(1 + \ln\left(1 + \rho_w^{-1} c_0^{-2} P\right)\right) S_0$ and (1.17) transforms to

$$\frac{\partial u}{\partial t} + \left(\alpha - \frac{1}{2}\right)\frac{\partial u^2}{\partial x} + (1+\varepsilon)\frac{1}{\rho}\frac{\partial P}{\partial x} = \psi \tag{1.18}$$

where

$$\varepsilon = (\alpha - 1)\frac{\rho}{\rho_w}\frac{S_0}{S}\left(\frac{u}{c_0}\right)^2 \frac{1}{1 + \rho_w^{-1} c_0^{-2} P}. \tag{1.19}$$

We note that for any velocity profile parameter $\gamma \geqslant 2$ the correction factor $\alpha \leqslant 4/3$ in (1.11) and (1.15). The physiology of arteries gives the estimates $\rho < \rho_w$, $S > S_0$, $u < 0.5$ m/s, $c_0 > 4$ m/s which guarantee that $\varepsilon < 5 \cdot 10^{-3}$. Under assumption that $\alpha$ is independent of $x$ one can omit the $\varepsilon$-term in (1.18) and approximate (1.18) by

$$\frac{\partial u}{\partial t} + \frac{\partial}{\partial x}\left(\left(\alpha - \frac{1}{2}\right)u^2 + \frac{P}{\rho}\right) = \psi. \tag{1.20}$$

For a rather flat profile ($\gamma = 9$, $\alpha = 1.1$), the contribution of the ignored $\varepsilon$-term in (1.18) is less than 0.16% $\left(\varepsilon < 1.6 \cdot 10^{-3}\right)$. Moreover, asymptotically $\varepsilon \to 0$ as $\alpha \to 1$ and (1.20) converges to (1.18) for almost flat profiles.

The 1D haemodynamic model (1.9), (1.11), (1.16) uses variables $(S, Q, P)$. In general this system is not hyperbolic. The 1D model (1.14), (1.20), (1.16) uses variables $(S, u, P)$. This formulation is appealing [5, 7, 11, 12, 28, 34, 35, 46] as it is hyperbolic and admits the divergent form which is useful for mathematical analysis and constructing efficient numerical methods. It is also possible to formulate a 1D haemodynamic model in $(R, P)$ variables closed by an elastic wall model [18].

### 1.2. 1D haemodynamic model for large deep veins

The systemic and pulmonary venous flows are necessary for modelling the closed-loop circulation, or global circulation, in the whole organism. The Reynolds number in veins ranges from 1 to $10^2$. The common approach is to use lumped compartment

models (Section 2), whereas haemodynamic 1D models are rarely used in this regard [8, 12, 28]. Usually, 1D models of venous blood flow adopt the 1D model for large arteries (Section 1.1) and modify the tube law. Such approach is valid for superficial veins as their walls have much common with arterial walls. Also, the approach is partly valid for deep veins in the standing position as they are smoothed out and their cross-section becomes circular. The cross-section of deep veins in the lateroprone position as well as other positions is elliptic or even dumbbell-shaped. Thus, the 1D haemodynamic model for large deep veins should account non-circular cross-sections.

**1.2.1. Averaging in elliptic cross-section.** In this section we confine ourselves by the elliptic cross-section with major and minor axes $a$ and $b$ which depend on $x$. The elliptic analogue of the circular profile (1.5) is

$$\xi_{ab}(y,z) = \frac{\gamma+2}{\gamma}\left(1-\left(\frac{y^2}{a^2}+\frac{z^2}{b^2}\right)^{\gamma/2}\right), \quad \frac{y^2}{a^2}+\frac{z^2}{b^2} \leqslant 1. \tag{1.21}$$

Similarly to (1.5) it produces a Poiseuille-like parabolic profile for $\gamma = 2$ and an almost flat profile for $\gamma = 9$:

$$u(t,x,y,z) = \bar{u}(t)\xi_{ab}(x,y,z). \tag{1.22}$$

Integration and averaging of the Navier–Stokes equations over a slice with an elliptic cross-section produce the same mass and momentum conservation equations (1.9), (1.11) with possibly different factors $\alpha$ and $K_r$ as they depend on the velocity profile (1.21). Using the polar coordinates $y = ra\cos\varphi$, $z = rb\sin\varphi$ ($0 \leqslant r \leqslant 1$, $0 \leqslant \varphi < 2\pi$) we have the same result (1.13) for the value of $\alpha$. The averaging of the friction term in (1.2) is modified as follows

$$-\nu\int\limits_{\Omega}\Delta u_x\,d\mathbf{x} = \nu\int\limits_{\partial\Omega}\nabla u_x\cdot\mathbf{n}\,ds = \nu u\int\limits_{\Gamma_W}\left(\frac{\partial\xi_{ab}}{\partial y}n_y+\frac{\partial\xi_{ab}}{\partial z}n_z\right)\mathrm{d}s \tag{1.23}$$

where from (1.21) we have

$$\left.\frac{\partial\xi_{ab}}{\partial y}\right|_{y^2/a^2+z^2/b^2=1} = -(\gamma+2)\frac{y}{a^2}, \quad \left.\frac{\partial\xi_{ab}}{\partial z}\right|_{y^2/a^2+z^2/b^2=1} = -(\gamma+2)\frac{z}{b^2} \tag{1.24}$$

and the outward normal to the elliptic wall is

$$\mathbf{n} = (n_y,n_z) = \left(\frac{y}{a^2\sqrt{\dfrac{y^2}{a^4}+\dfrac{z^2}{b^4}}}, \frac{z}{b^2\sqrt{\dfrac{y^2}{a^4}+\dfrac{z^2}{b^4}}}\right). \tag{1.25}$$

Finally we obtain

$$K_r = -\pi\nu(\gamma+2)\frac{a^2+b^2}{ab}. \tag{1.26}$$

For circular cross-sections we have $a = b$ and (1.26) reduces to (1.12).

**1.2.2. Constitutive relationship for elastic tubes with elliptic cross-section.** The constitutive relationship for a tube with elliptic cross-section is different from that for a tube with circular cross-section. For an elliptic ring with major and minor axes $a$ and $b$, we introduce eccentricity $k = \left(1-(b/a)^2\right)^{1/2}$ and wall thickness $h$. If we inflate the tube by internal pressure $P$, neglect axial effects and use the linear theory of deformations, then the strains along the major and minor axes $\delta_a$ and $\delta_b$ can be computed as [3]:

$$\delta_a = \frac{C_a a^4}{D}P, \quad \delta_b = \frac{C_b a^4}{D}P \tag{1.27}$$

where $D$ is the bending stiffness, coefficients $C_a$ and $C_b$ are

$$C_a = K_1\left(\frac{b^2}{2a^2}+\frac{b}{2ka}\arcsin k\right) - \frac{1-3k^2+2k^4}{16}+\frac{b}{16ka}\arcsin k \tag{1.28}$$

$$C_b = \frac{K_1}{2}+\frac{3k^2-1}{16}+\frac{b^2\left(8K_1+1+3k^3\right)}{32ka^2}\ln\frac{1+k}{1-k} \tag{1.29}$$

and $K_1$ is a constant. The tube law becomes

$$S = \pi(a+\delta_a)(b+\delta_b) = \pi a\left(b+(a+b)\frac{C_a a^3}{D}P+\frac{C_a C_b a^7}{D^2}P^2\right) = \hat{F}(P,a,b). \tag{1.30}$$

The solution of (1.30) gives the pressure $P$ as a function of the area $S$:

$$P = \frac{-B+\sqrt{B^2-4AC}}{2A} = F(S,a,b) \tag{1.31}$$

where $A = \pi C_a C_b a^8/D^2$, $B = \pi\,(a+b)\,C_a a^4/D$, $C = \pi ab - S$. We select the plus sign before the square root since the transmural pressure $P$ can be either negative or positive. The values $A$ and $B$ are always positive, thus $P>0$ for $S>\pi ab$ and $P<0$ for $\pi ab - \frac{1}{4}(a+b)^2 C_a/C_b < S < \pi ab$.

We note that

$$\frac{\partial \hat{F}}{\partial P} = \pi\frac{C_a a^4}{D}\left(a+b+\frac{C_b a^4}{D}P\right) \tag{1.32}$$

is a linear function of $P$. We also note, that for elliptic cross-sections the difference $S-S_0$ may be negative and positive. Thus the error of transforming (1.17) to (1.20) may be higher in this case.

## 2. Lumped haemodynamic models

Certain processes in the cardiovascular system do not rely on spatial effects of the nonlinear pulse wave propagation. For instance, microcirculation in microvasculature, transport of oxygen, carbon dioxide, drugs and nutrients, heart chambers

function may be imitated by lumped models. The lumped models relate the averaged haemodynamic parameters: pressure, flow and volume of the blood. Dynamic lumped models account time variability of the parameters, whereas stationary models relate the time-averaged values via nonlinear algebraic equations which may also include spatial derivatives. The latter models are useful for periodic or almost periodic haemodynamic processes with short transition periods.

Derivation of lumped models may be based on different principles. Here we derive dynamic (Section 2.1) and stationary (Section 2.2) lumped models from the 1D haemodynamic models for large arteries.

### 2.1. Dynamic lumped model

We consider an elastic tube with circular cross-section and length $l$ equal to its diameter. Rewriting the momentum equation (1.11), substituting the partial derivative $\partial/\partial x$ with its finite difference discretization with mesh size $\Delta x = l$, we get

$$\frac{\partial Q}{\partial t} + \frac{1}{\Delta x}\Delta\left(\alpha S^{-1}Q^2\right) + \frac{S}{\rho}\frac{\Delta P}{\Delta x} = K_r u. \tag{2.1}$$

Multiplying (2.1) by $\rho S^{-1}\Delta x$ and neglecting the change of the kinetic energy in the short tube we can transform (2.1) to

$$\rho S^{-1}\Delta x\frac{\partial Q}{\partial t} - \rho S^{-2}\Delta x K_r Q + \Delta P = 0. \tag{2.2}$$

We can rewrite (2.2) in the form

$$\frac{\rho l^2}{V}\frac{\mathrm{d}Q}{\mathrm{d}t} - \frac{\rho l^3 K_r}{V^2}Q + \Delta P = 0 \tag{2.3}$$

where $V = lS$ is the volume of the domain. Since $Q = \mathrm{d}V\mathrm{d}t$, we get finally

$$I\frac{\mathrm{d}^2V}{\mathrm{d}t^2} + R_h\frac{\mathrm{d}V}{\mathrm{d}t} + \Delta P = 0 \tag{2.4}$$

where the inertia coefficient $I$ and the hydraulic resistance $R$ are defined by

$$I = \frac{\rho l^2}{V}, \qquad R_h = 2\pi\nu\left(\gamma+2\right)\frac{\rho l^3}{V^2}. \tag{2.5}$$

We observe that coefficients $I$ and $R_h$ depend on the volume $V$, although in many works they are considered as constants [16, 39, 40]. Inertia effects are sometimes neglected ($I = 0$) [17]. It has proved that the solution by the lumped compartment approach for a vascular segment converges to the solution by 1D haemodynamic model for the same segment with the first order in space [26].

The momentum equation (2.4) may be applied to a spherical deformable element or to an arbitrary deformable convex element like a heart chamber. In the latter

case $\Delta P = P(V) - P_{\text{ext}} - P_{\text{ch}}$, where $P_{\text{ch}}$ is the pressure in the chamber, function $P(V)$ describes an elastic response of the chamber similar to the tube law for an elastic tube. The linear elasticity model of the heart chamber implies $P(V) = eV$, $e = \text{const}$, and $P_{\text{ext}}(t) < 0$ describes the pressure from myocardium contractions [16, 39]. The variable elasticity model of the heart chamber assumes $P(V) = P_0 + E(t)(V - V_0)$, $P_0 = \text{const}$, $V_0 = \text{const}$, and $E(t)$ is effective (average) elasticity due to the action-potential propagation through the myocardium, $P_{\text{ext}} = 0$ [17, 38, 42, 47].

The lumped model can account nonlinear effects via $I$, $R_h$ and $P(V)$. For instance, the blood rheology may be specified in $R$ (2.5) by a non-constant viscosity $\nu = \nu(Q)$. Viscoelasticity of the heart chambers may be introduced as $R_h = R_h(P)$ [24, 37, 43]. The heart rhythm variations are described by modifying $E(t)$ [13].

The momentum equation (2.4) may be also applied to a regional network of vessels. In this case $I$ is the effective inertia coefficient, $R_h$ is the effective hydraulic resistance, $E(t)$ is the effective elasticity. These coefficients are determined by fitting with experimental or clinical data or derived from the internal structure of the network (topological connectivity of its vessels). The latter reveals the electromechanical analogy between the lumped hydraulic compartments and electrical circuits. In this analogy the volume corresponds to the electric charge, the flow corresponds to the electric current, the inertia coefficient corresponds to the inductance, the hydraulic resistance corresponds to the electric resistance, the stiffness coefficient $e^{-1}$ corresponds to the capacity, the pressure corresponds to the electrical voltage [40]. The connection of several lumped hydraulic compartments is performed similarly to connections of elements of electrical circuits via the Kirchhoff's laws.

### 2.2. Stationary lumped model

The flow of viscous fluid is stationary in a tube with small diameter $d$ and length $\Delta x$. The Reynolds number lies in the range from $10^{-3}$ to 1, and one can neglect the flow acceleration $\partial Q/\partial t \approx 0$ and the change of the kinetic energy $\partial\left(\alpha Q^2/S\right)/\partial x \approx 0$ in order to derive from (2.1):

$$\frac{S}{\rho}\frac{\Delta P}{\Delta x} = K_r u \tag{2.6}$$

or, equivalently,

$$\Delta P = R_h Q, \qquad R_h = 2\mu(\gamma+2)\pi^{-1}d^{-4}\Delta x \tag{2.7}$$

where $R_h$ is the hydraulic resistance, $\mu = \nu\rho$ is the dynamic viscosity. For the parabolic profile ($\gamma = 2$ in (1.5)) we obtain the Poiseuille pressure drop condition. Model (2.7) considers microvasculature (arterioles, capillaries and venules) as a stationary lumped compartment. The microvessels are connected via the mass conservation condition at each junction point

$$\sum Q = 0. \tag{2.8}$$

Numerical models of blood flow in microvasculature based on (2.7), (2.8) are computationally expensive due to the nonlinear blood rheology and complex topological structure with $\sim 10^5$ microvessels per 1 cm$^3$ of the tissue. The models require solving systems of nonlinear algebraic equations.

The rheological properties of the blood are primary determined by the plasma viscosity, the volume fraction of the red blood cells (RBCs) (hematocrit), the RBC rheology, the RBC membrane elasticity, and interaction of RBCs. For various mathematical descriptions of the blood rheology we refer to [4, 29, 32, 33]. One possible way to account it is to define the hydraulic resistance as [40, 45]:

$$R_h = \frac{\pi \varkappa_1 d^4}{8\mu\Delta x}\left(1+\varkappa_2 Q^2\right) \tag{2.9}$$

with the predefined constants $\varkappa_1$ and $\varkappa_2$.

The topological structure of microvasculature may be recovered from high-resolution microcomputed tomography images [41]. A physiologically correct 3D structure may be imitated via a direct force repulsion–attraction nonlinear model [14]. Such structures are used in simulation of the transport of oxygen, drugs and other substances in spatially anisotropic models of the tumour growth [22] and the tissue perfusion.

## 3. Discussion

In the present paper we considered reduction of the Navier–Stokes equations to the 1D models of blood flow in arteries and veins, to the lumped dynamic compartment of regional arterial networks and heart chambers, and to the stationary compartment of microcirculation. We examined the limitations of the usage of variables ($S$, $u$, $P$) in the 1D models of arterial and venous flows. For tubes with elliptic cross-section, the analytic tube law was proposed. The relation between the lumped models parameters and mechanical and geometrical properties of the simulated structures was revealed. Boundary conditions for 1D haemodynamic models were not discussed in this paper, the interested reader is referred to [4, 20, 45].

Approximation (1.20) of (1.11) is based on small $\varepsilon$ in (1.18). We neglected the nonlinear term proportional to $(\varepsilon/\rho)\partial P/\partial x$ which may be large in some pathological conditions and may be important for a strict mathematical analysis of (1.9), (1.11). The exponential and the other analytic tube laws (their overview is given in [44]) provide bounded derivatives $\partial\hat{F}/\partial P$ in the neighbourhood of $S_0$, however, for veins we have linear dependence on $P$, $\partial\hat{F}/\partial P = O(P)$, and the thick wall approximation gives even sharper increase of $\partial\hat{F}/\partial P$ [21]. Therefore, simplification of (1.17) is valid for arteries whereas for veins it is valid just partly. Next, the formal asymptotics of (1.18) for $\gamma \to \infty$ results in the infinite viscosity term $\psi$ in (1.11) or (1.20) since it is proportional to $\gamma$. Thus the profile parameterization (1.5) is not suitable for such analysis. The other options for profile description are the power law profile and the Stokes layer [46]. Moreover, the actual velocity profile is not

constant in time that makes $\alpha$ to be a time-dependent function [30, 31]. The viscosity dependence on the flow velocity is typical for the venous and lymph flows [27]. Some approaches use more complicated Oldroyd viscoelastic fluid model [19].

Different physiological features of blood flows are not considered in this work. Accounting the arterial autoregulation, the heart and venous valves function, atherosclerotic plaques and endovascular implants modifies the considered 1D blood flow model [45].

## References


1. M. V. Abakumov, K. V. Gavrilyuk, N. B. Esikova, A. V. Lukshin, S. I. Mukhin, N. V. Sosnin, V. F. Tishkin, and A. P. Favorskii, Mathematical model of the hemodynamics of the cardio-vascular system, *Diff. Equations* **33** (1997), No. 7, 895–901.
2. D. Amadori, S. Ferrari, and L. Formaggia, Derivation and analysis of a fluid-dynamical model in thin and long elastic vessels. *Networks & Heterogeneous Media* **2** (2007), No. 1, 99–125.
3. R. T. Avery and G. A. Tidrick, Elliptical vacuum chamber stress and deflections. *IEEE Trans. Nuclear Science* **16** (1969), No. 3, 952–953.
4. N. Bessonov, A. Sequeira, S. Simakov, Yu. Vassilevski, and V. Volpert, Methods of blood flow modelling. *Math. Modelling Natur. Phenomena* **11** (2016), No. 1, 1–25.
5. E. Boileau, P. Nithiarasu, P. J. Blanco, L. O. Müller, F. E. Fossan, L. R. Hellevik, W. P. Donders, W. Huberts, M. Willemet, and J. Alastruey, A benchmark study of numerical schemes for one-dimensional arterial blood flow modelling. *Int. J. Numer. Meth. Biomed. Engrg.* **31** (2015), e02732.
6. A. G. Borzov, S. I. Mukhin, and N. V. Sosnin, Conservative schemes of matter transport in a system of vessels closed by the heart, *Diff. Equations* **48** (2012), No. 7, 919–928.
7. A. G. Borzov, S. I. Mukhin, and N. V. Sosnin, Conservative algorithm of substance transport over a closed graph of cardiovascular system. *Russ. J. Numer. Anal. Math. Modelling* **27** (2013), No. 5, 413–429.
8. A. Ya. Bunicheva, S. I. Mukhin, N. V. Sosnin, and A. B. Khrulenko, Mathematical modeling of quasionedimensional hemodynamics. *Comput. Math. & Math. Phys.* **55** (2015), No. 8, 1381–1392.
9. S. Čanić and E. H. Kim, Mathematical analysis of the quasilinear effects in a hyperbolic model blood flow through compliant axi-symmetric vessels. *Math. Meth. Appl. Sci.* **26** (2003), 1161–1186.
10. L. G. Fernandes, P. R. Trenhago, R. A. Feijóo, and P. J. Blanco, Integrated cardiorespiratory system model with short timescale control mechanisms, *Int. J. Numer. Meth. Biomed. Engrg.* (2019), e3332.
11. L. Formaggia, A. Quarteroni, and A. Veneziani, *Cardiovascular Mathematics: Modeling and Simulation of the Circulatory System, Vol. 1*. Springer, Heidelberg, 2009.
12. T. Gamilov, Y. Ivanov, Ph. Kopylov, S. Simakov, and Y. Vassilevski, Patient specific haemodynamic modeling after occlusion treatment in leg. *Math. Modeling Natur. Phenomena* **9** (2014), No. 6, 85–97.
13. T. Gamilov, Ph. Kopylov, M. Serova, R. Syunayaev, A. Pikunov, S. Belova, F. Liang, J. Alastruey, and S. Simakov, Computational analysis of coronary blood flow: the role of asynchronous pacing and arrhythmias. *Mathematics* **8** (2020), No. 8, 1205.
14. N. O. Gorodnova, A. V. Kolobov, O. A. Mynbaev, S. S. Simakov, Mathematical modeling of

blood flow alteration in microcirculatory network due to angiogenesis. *Lobachevskii J. Math.* **37** (2016), No. 5, 541–549.

15. R. Juodagalvytė, G. Panasenko, and K. Pileckas, Time periodic NavierStokes equations in a thin tube structure. *Boundary Value Problems* (2020), No. 2020, 28.
16. A. S. Kholodov, Some dynamical models of multi-dimensional problems of respiratory and circulatory systems including their interaction and matter transport. In: *Computer Models and Medicine Progress*. Nauka, Moscow, 2001, 127–163 (in Russian).
17. T. Korakianitis and Y. Shi, Numerical simulation of cardiovascular dynamics with healthy and diseased heart valves. *J. Biomechanics* **39** (2006), No. 11, 1964–1982.
18. V. A. Kozlov and S. A. Nazarov, Asymptotic models of the blood flow in arteries and veins. *J. Math. Sci.* **194** (2013), No. 1, 44–57.
19. V. A. Kozlov and S. A. Nazarov, One-dimensional model of viscoelastic blood flow through a thin elastic vessel. *J. Math. Sci.* **207** (2015), No. 2, 249–269.
20. V. A. Kozlov and S. A. Nazarov, A one-dimensional model of flow in a junction of thin channels, including arterial trees. *Sbornik: Mathematics* **208** (2017), No. 8, 1138–1186.
21. P. Kozlovsky, U. Zaretsky, A. J. Jaffa, and D. Elad, General tube law for collapsible thin and thick-wall tubes, *J. Biomechanics* **47** (2014), No. 10, 2378–2384.
22. M. B. Kuznetsov, N. O. Gorodnova, S. S. Simakov, and A. V. Kolobov, Multiscale modeling of angiogenic tumor growth, progression, and therapy, *Biophysics* **61** (2016), No. 6, 1042-1051.
23. F. Liang and H. Liu, A closed-loop lumped parameter computational model for human cardiovascular system. *JSME Int. J., Series C: Mechanical Systems, Machine Elements and Manufacturing* **48** (2006), No. 4, 484–493.
24. F. Liang, S. Takagi, R. Himeno, and H. Liu, Multi-scale modeling of the human cardiovascular system with applications to aortic valvular and arterial stenoses. *Medical & Biological Engrg. & Computing* **47** (2009), 743–755.
25. A. Lozovskiy, M. Olshanskii, and Y. Vassilevski, Analysis and assessment of a monolithic FSI finite element method. *Computers & Fluids* **179** (2019), 277–288.
26. V. Milisic and A. Quarteroni, Analysis of lumped parameter models for blood flow simulations and their relation with 1D models. *ESAIM: Mathematical Modelling and Numerical Analysis* **38** (2004), No. 4, 613–632.
27. A. S. Mozokhina and S. I. Muhin, Quasi-one-dimensional flow of a fluid with anisotropic viscosity in a pulsating vessel. *Diff. Equations* **54** (2018), No. 7, 956-962.
28. L. O. Müller and E. Toro, A global multiscale mathematical model for the human circulation with emphasis on the venous system. *Int. J. Numer. Meth. Biomed. Engrg.* **30** (2014), No. 7, 681–725.
29. A. S. Popel and P. C. Johnson, Microcirculation and hemorheology. *Ann. Rev. Fluid Mechanics* **37** (2005), 43–69.
30. I. Sazonov, S.-Y. Yeo, R. L. T. Bevan, P. Nithiarasu, R. van Loon, and X. Xie, A robust subject-specific modelling pipeline for arterial blood flow dynamics — a review. *Int. J. Numer. Meth. Biomed. Engrg.* **27** (2011), No. 8, 1167–1184.
31. I. Sazonov and P. Nithiarasu, A novel, FFT-based one-dimensional blood flow solution method for arterial network. *Biomechanics and Modelling in Mechanobilogy* **18** (2019), 1311–1334.
32. T. W. Secomb, Hemodynamics. *Comprehensive Physiology* **6** (2016), No. 2, 975–1003.
33. T. W. Secomb, Blood flow in the microcirculation. *Ann. Rev. Fluid Mechanics* **49** (2017), 443–461.

34. S. J. Sherwin, V. Franke, J. Peiró, and K. Parker, One-dimensional modelling of a vascular network in space-time variables. *J. Engrg. Mathematics* **47** (2003), 217–250.

35. S. J. Sherwin, L. Formaggia, J. Peiró, and V. Franke, Computational modelling of 1D blood flow with variable mechanical properties and its application to the simulation of wave propagation in the human arterial system. *Numer. Meth. Fluids* **43** (2003), 673–700.

36. Y. Shi, P. Lawford, and R. Hose, Review of zero-D and 1-D models of blood flow in the cardiovascular system. *BioMedical Engineering OnLine* **10** (2011), No. 1, 33.

37. S. G. Shroff, J. S. Janicki, and K. T. Weber, Evidence and quantitation of left ventricular systolic resistance. *American J. Physiology-Heart and Circulatory Physiology* **249** (1985), No. 2, H358–H370.

38. S. S. Simakov, Lumped parameter heart model with valve dynamics. *Russ. J. Numer. Anal. Math. Modelling* **34** (2019), No. 5, 289–300.

39. S. S. Simakov and A. S. Kholodov, Computational study of oxygen concentration in human blood under low frequency disturbances. *Math. Models Computer Simulations* **1** (2009), No. 2, 283–295.

40. S. S. Simakov, Modern methods of mathematical modeling of blood flow using reduced order methods. *Computer Research and Modeling* **10** (2018), No. 5, 581–604 (in Russian).

41. S. K. Stamatelos, E. Kim, A. P. Pathak, and S. P. Aleksander, A bioimage informatics based reconstruction of breast tumor microvasculature with computational blood flow predictions. *Microvasc. Research* **91** (2014), 8–21.

42. H. Suga, Cardiac energetics: from $E_{MAX}$ to pressure-volume area. *Clinical and Experimental Pharmacology and Physiology* **30** (2003), No. 8, 580–585.

43. Y. Sun, M. Beshara, R. J. Lucariello, and S. A. Chiaramida, A comprehensive model for right-left heart interaction under the influence of pericardium and baroreflex. *American J. Physiology* **272** (1997), H1499–H1515.

44. Yu. V. Vassilevski, V. Y. Salamatova, and S. S. Simakov, On the elasticity of blood vessels in one-dimensional problems of hemodynamics. *Comput. Math. & Math. Phys.* **55** (2015), No. 9, 1567–1578.

45. Yu. Vassilevski, M. Olshanskii, S. Simakov, A. Kolobov, and A. Danilov, *Personalized Computational Hemodynamics: Models, Methods, and Applications for Vascular Surgery and Antitumor Therapy*. Academic Press, London–San Diego–Cambridge–Oxford, 2020.

46. F. N. van de Vosse and N. Stergiopulos, Pulse wave propagation in the arterial tree. *Annual Review of Fluid Mechanics* **43** (2011), 467–499.

47. K. R. Walley, Left ventricular function: time-varying elastance and left ventricular aortic coupling. *Critical Care* **20** (2016), No. 270, 1–11.